Ultrasound in Med. & Biol., Vol. 00, No. 00, pp. 1–8, 2019

0301-5629/$ - see front matter

https://doi.org/10.1016/j.ultrasmedbio.2019.06.004

● *Technical Note*

COMBINED CONFOCAL MICROSCOPE AND BRANDARIS 128 ULTRA-HIGH-SPEED CAMERA

Inés Beekers,* Kirby R. Lattwein,* Joop J.P. Kouijzer,* Simone A.G. Langeveld,* Merel Vegter,* Robert Beurskens,* Frits Mastik,* Rogier Verduyn Lunel,† Emma Verver,‡ Antonius F.W. van der Steen,*,§ Nico de Jong,*,§ and Klazina Kooiman*

* Department of Biomedical Engineering, Thoraxcenter, Erasmus MC, Rotterdam, The Netherlands; † Nikon Instruments Europe, Amsterdam, The Netherlands; ‡ Nikon Netherlands, Amsterdam, The Netherlands; and § Laboratory of Acoustical Wavefield Imaging, Delft University of Technology, Delft, The Netherlands

(*Received* 19 *March* 2019; *revised* 23 *May* 2019; *in final from* 5 *June* 2019)

Abstract—Controlling microbubble-mediated drug delivery requires the underlying biological and physical mechanisms to be unraveled. To image both microbubble oscillation upon ultrasound insonification and the resulting cellular response, we developed an optical imaging system that can achieve the necessary nanosecond temporal and nanometer spatial resolutions. We coupled the Brandaris 128 ultra-high-speed camera (up to 25 million frames per second) to a custom-built Nikon A1R+ confocal microscope. The unique capabilities of this combined system are demonstrated with three experiments showing microbubble oscillation leading to either endothelial drug delivery, bacterial biofilm disruption, or structural changes in the microbubble coating. In conclusion, using this state-of-the-art optical imaging system, microbubble-mediated drug delivery can be studied with high temporal resolution to resolve microbubble oscillation and high spatial resolution and detector sensitivity to discern cellular response. Combining these two imaging technologies will substantially advance our knowledge on microbubble behavior and its role in drug delivery. (E-mail: d.beekers@erasmusmc.nl) **© 2019 The Author(s). Published by Elsevier Inc. on behalf of World Federation for Ultrasound in Medicine & Biology. This is an open access article under the CC BY-NC-ND license. (http://creativecommons.org/licenses/by-nc-nd/4.0/).**

Key Words: **Bacteria, Confocal microscopy, Drug delivery, Fluorescence microscopy, High-speed imaging, Lipid coating, Microbubble, Sonoporation, Ultrasound, Ultrasound contrast agents.**

INTRODUCTION

To successfully treat diseases, administered drugs need to overcome barriers in the human body that hinder efficient delivery. Currently, high dosages are required because only a fraction of the therapeutic actually reaches the target site. This leads to high toxicity levels in healthy tissue, causing undesirable side effects (Binsalamah et al. 2012; Westein et al. 2013). However, lipid-coated gas microbubbles (1–10 μm) in combination with ultrasound can locally enhance drug delivery, allowing for therapeutics to be delivered efficiently and only to the intended target site. When ultrasound is applied, microbubbles oscillate and thereby permeabilize cell membranes (sonoporation), open intercellular junctions, and stimulate endocytosis (Kooiman et al. 2014b; Lentacker et al. 2014; Qin et al. 2018). The underlying physical and biological mechanisms enhancing these different pathways are poorly understood. Elucidating the microbubble–cell interaction is fundamentally important for controlling and optimizing drug delivery, and therefore, microbubble oscillation behavior and the cellular response should be studied simultaneously.

To resolve the microbubble oscillation in an ultrasound field of clinically relevant frequencies (MHz), a system with nanosecond temporal resolution is required. Currently, there are two ultra-high-speed cameras that can achieve such high frame rates, up to 25 million frames per second (Mfps) with sufficient consecutive frames: the Brandaris 128 (Chin et al. 2003) and the UPMC Cam (Chen et al. 2013). Both cameras have been coupled to an upright microscope (BXFM, Olympus, Tokyo, Japan) for brightfield and widefield fluorescence microscopy. This enables the concurrent visualization of microbubble oscillation and cellular response. Although these systems have been used to study vascular drug delivery (Helfield et al.

Address correspondence to: Inés Beekers, Office Ee2302, PO Box 2040, 3000 CA Rotterdam, The Netherlands. E-mail: d.beekers@erasmusmc.nl

2016, 2017; Kooiman et al. 2011; van Wamel et al. 2006), imaging resolution showing the cellular response was very poor. Microbubble oscillation leading to bacterial biofilm disruption has been observed at a lower temporal resolution using a 3 Mfps camera (Goh et al. 2015). With the use of high-speed cameras, it has been possible to study the microbubble–cell interaction; however, the cellular response was still imaged with poor sensitivity and at a low optical and temporal resolution.

Confocal microscopy allows us to better unravel cellular response, as it provides nanometer spatial resolution, 3-D imaging with high axial resolution, and good detector sensitivity for different fluorescent cell labeling. Live confocal microscopy imaging of microbubble-mediated drug delivery has revealed a wide-range of cellular effects: pore formation (Fan et al. 2012) and recovery (Hu et al. 2013), opening of intercellular junctions (Helfield et al. 2016), endocytosis (De Cock et al. 2015), lipoplex (Lentacker et al. 2009) and doxorubicin (Lentacker et al. 2010) delivery, changes in reactive oxygen species levels (Jia et al. 2018), increased bacterial metabolism (Hu et al. 2018), sonoprinting (De Cock et al. 2016), cytoskeleton disruption (Chen et al. 2014), and intercalation of model drugs (Lammertink et al. 2017). However, all these studies lack information on the specific microbubble behavior that was responsible for the observed cellular effect, because of the relatively low frame rates of confocal microscopy imaging (<500 fps).

Microbubble response to ultrasound varies a lot, and even equal-sized microbubbles in the same ultrasound field do not respond identically (Emmer et al. 2009; Helfield et al. 2012; Maresca et al. 2010). We need to gain more insight into microbubble behavior to achieve a more predicable response to ultrasound. To understand how the response is affected by microbubble composition, we want to image both the microbubble oscillation behavior and the coating microstructure (Kwan and Borden 2012). In the past, it has only been possible to image coating microstructure in a static setup, without ultrasound, using, for example, 4Pi high-resolution confocal microscopy (Kooiman et al. 2014a).

To date, the technological gap has made it impossible to image microbubble oscillation (high temporal resolution) and detailed cellular response (high spatial resolution) in the same field of view of a single sample. To overcome this challenge, we developed a novel optical imaging system by coupling an upright custom-built Nikon confocal microscope to the Brandaris 128 ultra-high-speed camera (Fig. 1), which is described in this technical note.

METHODS

The Brandaris 128 ultra-high-speed camera is a programmable camera with 128 sensitive charge-coupled devices (CCDs) and a fast rotating mirror that sweeps the image over the CCDs, resulting in a minimum interframe time of 40 ns (25 Mfps) (Chin et al. 2003). Consecutive 128-frame recordings can be done at an 80 ms interval, with a maximum of 50 consecutive recordings (Gelderblom et al. 2012). The brightfield image is 500 × 292 pixels with 8-bit gray-scale values and a typical resolution of 400 nm (Chin et al. 2003).

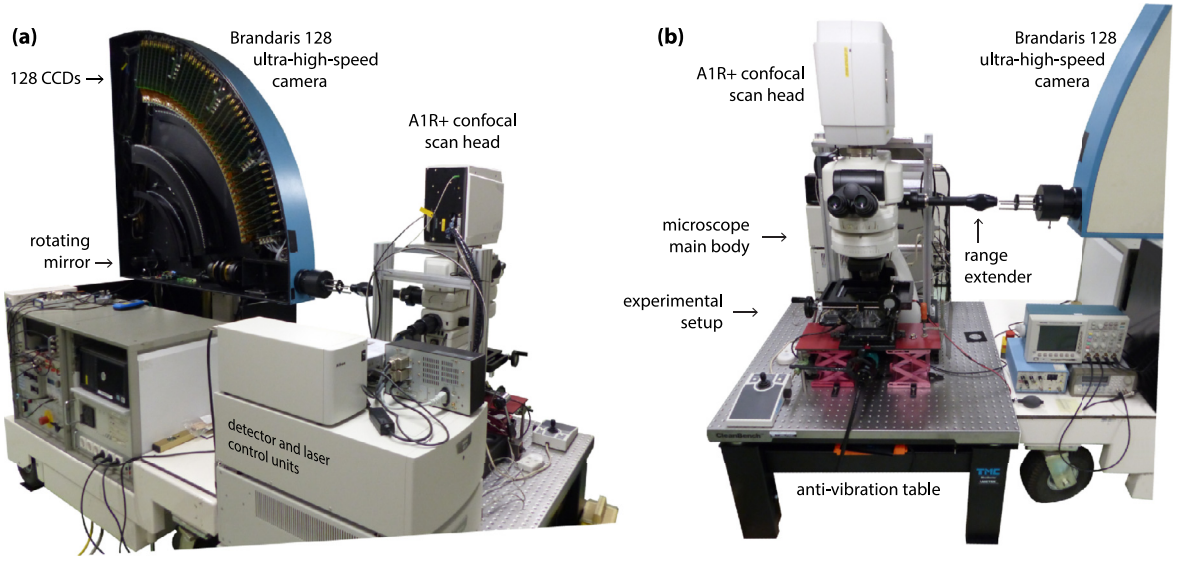

Fig. 1. Combined confocal microscope and Brandaris 128 ultra-high-speed camera. (a) From the back of the system, the inside of the Brandaris 128 casing with the rotating mirror and 128 charge-coupled devices (CCDs) is seen. (b) At the front of the system are the confocal microscope and the experimental setup. The range extender facilitates the coupling of the Brandaris 128 to the confocal microscope.

The main body of the confocal microscope is a custom-built upright Eclipse Ni-E microscope (Nikon Instruments, Amsterdam, The Netherlands). By physically removing the conventional base of the main body, the microscope was customized to accommodate the water bath for ultrasound insonification. Microscope modules were chosen to meet our requirements such that the light path (Fig. 2) could be directed toward the four different output ports: (i) a binocular (NI-TT-E Motorized Quadrocular Tilting Tube, Nikon Instruments), (ii) a color camera (DS-Fi3, Nikon Instruments) for digital acquisition of brightfield and widefield fluorescence images, (iii) the A1R+ confocal scan head, and (iv) the Brandaris 128 ultra-high-speed camera.

Two motorized turret modules (NI-FLT6-E Mot Epi-fluorescent turret, Nikon Instruments) were incorporated to rotate the desired filters or mirrors into the light path. One turret holds a full mirror to direct the light path toward the Brandaris 128 camera (Fig. 2, *turret A*). The other turret is used for switching between filter cubes for widefield fluorescence imaging (Fig. 2, *turret B*). The four installed filter cubes have the following emission (Em), dichroic mirror (DM), and excitation (Ex) filters: BFP-A with Em390/18, DM416, and Ex460/60; GFP-A with Em469/35, DM497, and Ex525/39; TRITC-A with Em542/20, DM570, and Ex620/52; and Cy5-4040 C with Ex628/40, DM660, and Em692/40 (center wavelength/bandwidth in nanometers; Semrock Inc., Rochester, NY, USA). Widefield fluorescence is performed with a metal halide light source with motorized shutters and neutral density filters (C-HGFIE, Fiber Illuminator Intensilight, Nikon Instruments). During confocal imaging, excitation is achieved with a laser unit (LU-N4, Nikon Instruments) equipped with four lasers (405, 488, 561, and 640 nm; all 15 mW at the output of the fiber tip). The system has a hybrid detector unit (A1-DUG, GaAsP Multi Detector Unit, Nikon Instruments) that includes two gallium arsenide phosphide (GaAsP) photomultiplier tubes (PMTs) and two standard multi-alkali PMTs. The GaAsP PMTs are highly efficient in detecting the 525/50 and 595/50 nm ranges in comparison to the standard multi-alkali PMTs. To create four detection channels, the emitted light is split using three filter cubes. The first filter cube (DM FF495-Di03, Semrock Inc.; Em filter ET450/50 m, Chroma, Bellows Falls, VT, USA) delimits the 450/50 nm channel which is detected by a standard multi-alkali PMT. The second filter cube (DM T560 LPXR, Chroma; Em filter ET525/50 m, Chroma) delimits the 525/50 nm channel, which is detected by a GaAsP PMT. The third filter cube (DM T640 LPXR, Chroma; Em filter ET595/50 m, Chroma; Em ET700/75 m, Chroma) delimits the 595/50 and 700/75 nm channels, which are detected with a GaAsP PMT and a standard multi-alkali PMT, respectively.

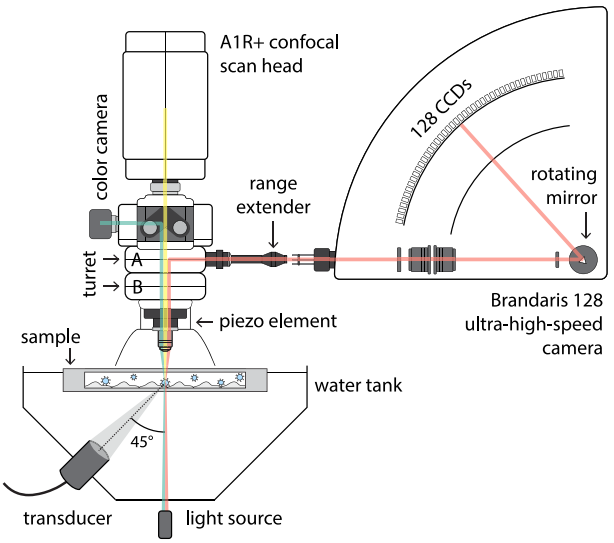

Fig. 2. Schematic of the light paths to the different imaging output ports (not to scale). The light path goes through the sample, the objective, and the main body of the microscope toward either the color camera (*green*), the confocal scan head (*yellow*) or the Brandaris 128 ultra-high-speed camera (*red*). The light source is used for brightfield and Brandaris 128 imaging. The motorized turret A can place the full mirror in the light path for Brandaris 128 imaging, while turret B can insert the desired filter cubes for widefield fluorescence imaging. The sample can be insonified from below under a 45° angle in a water tank, which can be heated to 37°C. CCDs = charge-coupled devices.

For high-precision focusing and 3-D z-stack imaging, the microscope's main body combines two z-scanning devices. First, long ranges (12 mm) can be scanned with the main body's motorized z functionality, which was retained despite the customization. Next, with a piezo element (MCL NANO-F200 N, Mad City Labs Inc., Madison, WI, USA), faster and more precise z-focusing can be performed in a 200 μm range, resulting in improved *z*-stack imaging. To isolate vibration, the confocal microscope was installed on an active anti-vibration optical table (74-9090 M Cleanbench top and 12M-424-88 micro-g modular post mount support, Physik Instrumente, Karlsruhe, Germany).

The field of view of the Brandaris 128 camera had to overlap with that of the microscope. Therefore, the Brandaris 128 camera's casing had to be aligned and coupled to the output port of the microscope's main body. This was achieved by fixing a laser pointer on the casing of the Brandaris 128 to project onto a target on the microscope body. Further, to reproduce alignment, the position of both systems with respect to the room was documented using a laser distance measuring tool (GLM 40, Bosch, Stuttgart, Germany). A second requirement was parfocality; that is, the Brandaris 128 and the confocal need to have the same focal plane. To that end, a range extender (XT2 Collimating

Emission-Port Adaptor, Photometrics, Tucson, AZ, USA) was inserted in the light path between the output port of the microscope and the Brandaris 128 input port.

When fast switching between confocal imaging and Brandaris 128 acquisition is desired, a Multifunction I/O Device (USB-6000, National Instruments, Austin, TX, USA) can trigger the motorized turret to rotate the full mirror into the light path, temporarily intercepting time-lapse confocal imaging to acquire with the Brandaris 128 camera instead. The trigger is given when the rotating mirror in the Brandaris 128 reaches a desired rotation speed. Once the Brandaris 128 acquisition is complete, another trigger is given to remove the mirror from the light path, such that confocal imaging is restored. The confocal recording is intercepted at least for the duration of consecutive Brandaris 128 recordings and the mechanical turret rotation time of 300 ms. The trigger events and turbine speeds are registered in the confocal recording for correct data registration.

The capabilities of the combined Brandaris 128 and confocal microscopy imaging system are demonstrated with three *in vitro* experiments: endothelial drug delivery, bacterial biofilm disruption, and microbubble coating microstructure alterations. The microbubbles used in the experiments were all in-house produced by probe sonication as previously described (Kooiman et al. 2014a). Briefly, the main lipid of the coating was 1,2-distearoyl-*sn*-glycero-3-phosphocholine and the microbubbles had a C_4F_{10} gas core. All images were acquired with a 100 × objective (CFI Plan 100XC W, Nikon Instruments) that is chromatic aberration-free infinity (CFI), corrected for field curvature (Plan) and water dipping (W). This objective has a numerical aperture of 1.10; therefore, the resolution achieved with confocal microscopy is 250 nm. The confocal scan speed varies from 0.03−1 fps per acquisition channel, depending on the chosen pixel dwell time. By decreasing the field of view, we can image up to 5 fps. From the Brandaris 128 ultra-high-speed recordings, the microbubble radius as function of time was determined using custom-designed image analysis software (van der Meer et al. 2007). During the endothelial drug delivery and biofilm disruption experiments, the sample was inserted in the water tank at 37°C (Fig. 2) and insonified with a single-element focused transducer (2.25 MHz center frequency, 76.2 mm focal length, −6 dB beam width at 2 MHz of 3 mm; V305, Panametrics-NDT, Olympus, Waltham, MA, USA). When the microbubble coating was studied, the sample was inserted in the water tank at room temperature and insonified with a single-element broadband transducer (1 to 9 MHz bandwidth, 25 mm focal distance, −6 dB beam width at 1 MHz of 1.3 mm; PA275, Precision Acoustics, Dorchester, U.K.).

RESULTS

In the first experiment, the response of human umbilical vein endothelial cells to $\alpha_v\beta_3$-targeted microbubbles upon ultrasound insonification was imaged. Acquisition started with confocal microscopy time-lapse imaging (0.65 fps, CFI Plan 100 × W objective), revealing the initial state of the cells and the location of the microbubble (Fig. 3a). Next, the light path was automatically switched toward the Brandaris 128 to record microbubble oscillation during ultrasound insonification (2 MHz, 250 kPa peak-negative-pressure [PNP], single 10-cycle burst) (Fig. 3b). This temporarily intercepted confocal microscopy imaging until the Brandaris 128 recording finished and the light path was switched back. Confocal microscopy imaging proceeded for 3.5 min after ultrasound, monitoring the cellular response (Fig. 3c). Uptake of propidium iodide was observed locally around the microbubble (Fig. 3c, 00:30−00:44), followed by diffusion throughout the cytoplasm and into the nucleus (Fig. 3c, 02:25). Moreover, confocal microscopy imaging revealed opening of the intercellular junctions (Fig. 3c, 02:25−03:50, *arrows*).

The second experiment started with confocal microscopy time-lapse imaging (0.32 fps, CFI Plan 100 × W objective) of a *Staphylococcus aureus* biofilm. This revealed vancomycin-targeted microbubbles adhered to bacteria (Fig. 4a). Confocal time-lapse imaging was temporarily intercepted to record microbubble oscillation with the Brandaris 128 upon ultrasound insonification (2 MHz, 250 kPa PNP, single 10,000-cycle burst). After the Brandaris 128 recording, the light path was switched back and confocal imaging continued for 40 s. Confocal microscopy imaging after insonification revealed microbubbles had clustered (Fig. 4c). Moreover, bacteria detached in the area where microbubbles were originally located, revealing microbubble-mediated disruption of the biofilm (Fig. 4c, 0:22, *arrows*). Toward the end of the confocal recording, partial redisposition of bacteria was observed (Fig. 4c, 00:57).

The third experiment aimed to image the microbubble coating microstructures before and after ultrasound insonification. Before ultrasound, a *z*-stack was acquired (0.4 μm step size, 31 slices, CFI Plan 100 × W objective) of a microbubble that also contained rhodamine-B-1, 2-dihexadecanoyl-*sn*-glycero-3-phosphoethanolamine, triethylammonium salt (rhodamine-DHPE). The 3-D image (Fig. 5a) revealed that the lipid expanded phase, as stained by the rhodamine-DHPE (Baumgart et al. 2007), was distributed in a characteristic honeycomb pattern. Next, Brandaris 128 ultra-high-speed imaging revealed microbubble oscillation (Fig. 5b) upon ultrasound insonification (1.4 MHz, 50 kPa PNP, single 8-cycle burst). After ultrasound, another *z*-stack was acquired revealing structural changes in the microbubble coating (Fig. 5c, *arrows*).

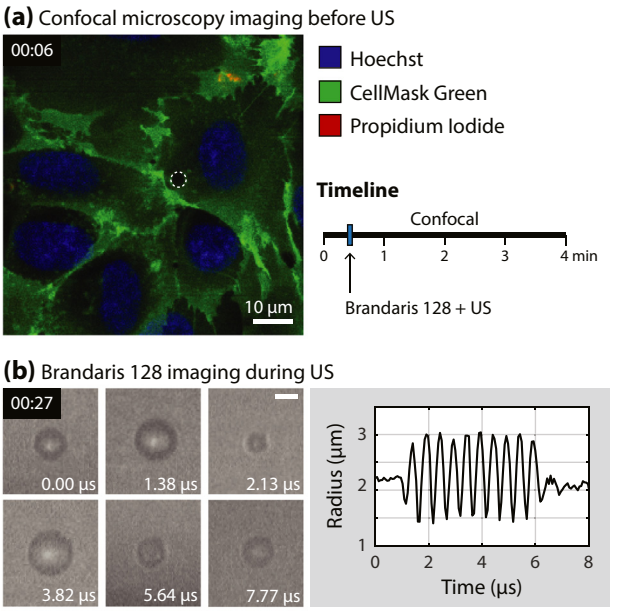

Fig. 3. Selected frames from time-lapse imaging of microbubble-mediated endothelial drug delivery. Human umbilical vein endothelial cells (Lonza, Verviers, Belgium) were grown in MV2 medium (PromoCell GmbH, Heidelberg, Germany) to confluency for 2 d in a CLINIcell (50 μm membrane; Mabio, Turcoing, France). The cell nuclei were stained with Hoechst (5 μg/mL; Thermo Fisher Scientific, Waltham, MA, USA), the cell membranes with CellMask Green (4 μg/mL; Thermo Fisher Scientific), and sonoporation with propidium iodide (25 μg/mL; Sigma-Aldrich, St. Louis, MO, USA). The *dashed line* delineates the microbubble. (a) Confocal microscopy before ultrasound (US) to image the initial cell state. (b) Microbubble oscillation recorded with the Brandaris 128 ultra-high-speed camera (bar = 3 μm) and the microbubble radius as a function of time determined from this recording. (c) Confocal microscopy after US to image cellular response. The *arrows* indicate opening of intercellular junctions.

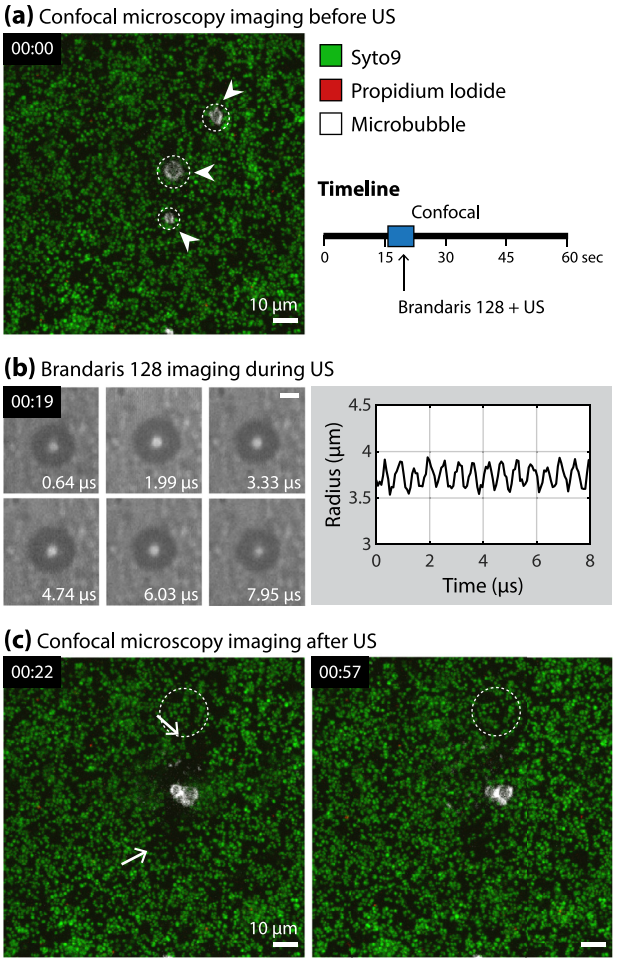

Fig. 4. Selected frames from time-lapse imaging of microbubble-mediated biofilm disruption. A clinical isolate of *Staphylococcus aureus* (SA25268) was grown in IMDM medium (Thermo Fisher Scientific) for 24 h in an ibiTreat μ-slide (0.8 mm channel height; I Luer; Ibidi GmbH, Martinsried, Germany). The live bacteria were stained with SYTO 9 (4 μg/mL; Thermo Fisher Scientific), the dead bacteria with propidium iodide (25 μg/mL; Sigma-Aldrich) and the microbubble shell with DiD (Thermo Fisher Scientific). (a) Confocal microscopy before ultrasound (US) to image the initial biofilm and microbubbles (*arrowheads*). (b) The oscillation of the microbubble located in the center of (a) was recorded with the Brandaris 128 ultra-high-speed camera (bar = 3 μm). The microbubble radius as a function of time was extracted from this recording. (c) Confocal microscopy after US to image biofilm disruption (*arrows*).

DISCUSSION

The novel combined confocal microscope and Brandaris 128 ultra-high-speed camera make it possible to study both the cell and microbubble structures with nanometer spatial resolution and the microbubble oscillation with nanosecond temporal resolution, as demonstrated with the three experiments. With this unique device we were able for the first time to relate

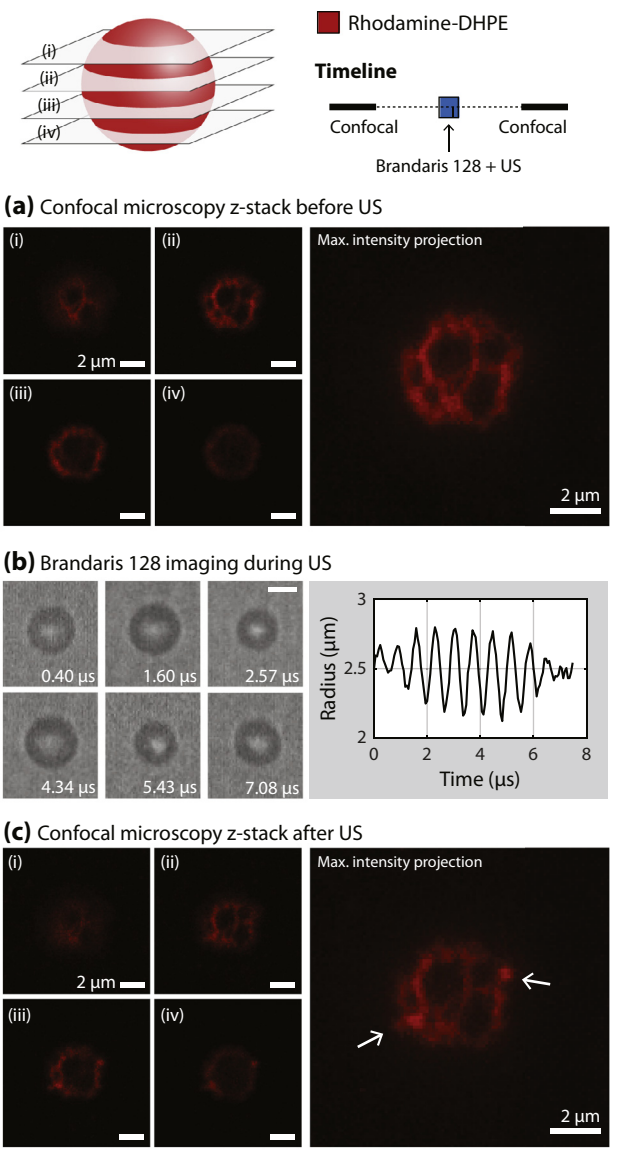

Fig. 5. Imaging of structural changes in microbubble coating. The lipid-expanded phase was stained with rhodamine-DHPE (0.01 mol%; Thermo Fisher Scientific). Microbubbles were studied in a CLINIcell (50 μm membrane; Mabio). (a) Selected *z*-slices from 3-D confocal microscopy (i–iv) and the maximum intensity projection before ultrasound (US). (b) Selected frames of the Brandaris 128 ultra-high-speed recording revealing microbubble oscillation (bar = 3 μm) and the resulting microbubble radius as a function of time. (c) Selected *z*-slices (i–iv) and maximum intensity projection after US. The *arrows* indicate a focal area of increased fluorescence intensity (*i.e.,* hot spot) suggestive of local microbubble shell buckling.

microbubble oscillation behavior to alterations in cell integrity and microbubble coating microstructures.

Microbubble-mediated endothelial drug delivery (Fig. 3) monitored with confocal microscopy provides better detector sensitivity and higher frame rates than the widefield microscope originally coupled to the Brandaris 128. As a result, low and fast changes of local propidium iodide uptake caused by sonoporation can now be detected. This is essential when studying safe drug delivery because low uptakes have been associated with reversible sonoporation and cell viability (van Rooij et al. 2016). Moreover, specific fluorescent cell dyes can now be imaged with high resolution, revealing previously concealed cellular responses. For example, we were able to observe the opening of intercellular junctions using a cell membrane dye (Fig. 3c).

The advantage of high-resolution confocal microscopy is also demonstrated when imaging biofilm disruption by oscillating microbubbles (Fig. 4). Because of the small size of bacteria ($\sim$1 μm in diameter), they cannot be well resolved with widefield microscopy. The added value of this new optical system is that we can now distinguish individual bacteria and observe effects on biofilms caused by oscillating microbubbles, while also gaining insight into how microbubbles vibrate nearby a biofilm. Furthermore, the light path switching is quick enough to observe the disruption of the biofilm before redisposition of bacteria occurs (Fig. 4c). However, this data set also reveals a drawback of the Brandaris 128 ultra-high-speed camera recordings. Because a maximum of 128 frames can be acquired, it is only possible to partially image the 10,000-cycle microbubble oscillation. Therefore, in this Brandaris 128 acquisition, the microbubble clustering was not observed (Fig. 4b) and could only be inferred from the confocal microscopy after ultrasound (Fig. 4c).

The developed optical imaging system will be essential not only in understanding ultrasound-mediated drug delivery, but also in designing ultrasound contrast agents. We can finally image how microbubble oscillation behavior affects the structural organization of the coating and vice versa. Although 4Pi microscopy has higher axial resolution and overcomes the signal loss toward the part of the microbubble furthest away from the objective (Fig. 5, iv), because of the laser diffraction by the microbubble's gas core, we were able to discern the coating microstructures with the confocal microscope (Fig. 5). To date, lipid shedding and buckling of the phospholipid shell caused by microbubble oscillation has been observed only using widefield fluorescence microscopy, at 150,000 fps (Luan et al. 2014) or 5 Mfps (Kooiman et al. 2017). However, because of the poor axial resolution of widefield microscopy, structural details of the phospholipid shell could not be resolved.

Simultaneous Brandaris 128 and confocal microscopy imaging is not possible with the combined system. This technical limitation remains as the Brandaris 128 requires 100% of the light path to overcome the CCD detection limits. Automatic switching between confocal and Brandaris 128 imaging minimizes the time during

which confocal microscopy imaging is interrupted. It is difficult to precisely predict the start of a Brandaris 128 acquisition, as the acceleration of the turbine is variable. Therefore, confocal microscopy is often interrupted about 2 s before the Brandaris 128 recording starts. During this time no change is expected in the confocal image, because insonification has not taken place yet. As soon as the Brandaris 128 acquisition has completed, during which ultrasound was applied, the full mirror is rotated out of the light path. As a result, the confocal microscope can restore imaging to detect rapid cellular effects with a maximum delay of 300 ms plus the time to scan a confocal frame (which depends on the confocal scan speed chosen). For the endothelial drug delivery example, this corresponded to <1.8 s, and for the biofilm disruption example, this was <3.4 s.

The confocal microscope can image a larger field of view than the Brandaris 128 ultra-high-speed camera. For instance, with the CFI Plan 100 × W objective, the field of view of the confocal microscope is 128 × 128 μm and that of the Brandaris 128 is 45 × 32 μm. Hence, as seen in Figure 4, sometimes microbubbles are observed in the field of view of the confocal microscope, but their oscillation cannot be recorded with the Brandaris 128. Finally, adapting the microscope's main body by removing the conventional base disabled the automatic refocusing capability. Regardless, a desired focus depth can be manually restored because the software is still able to read out the *z*-position of the objective.

CONCLUSIONS

A state-of-the-art optical imaging system was developed by coupling a custom-built confocal microscope to the Brandaris 128 ultra-high-speed camera. Microbubble-mediated drug delivery can now be studied at both high spatial and temporal resolution to evaluate cellular response upon microbubble oscillation. Additionally, changes in microbubble coating structure caused by oscillation behavior can be discerned. With this novel optical imaging system we expect to further elucidate microbubble-mediated drug delivery and advance the development of ultrasound contrast agents.

Acknowledgments—This work was supported in part by the Applied and Engineering Sciences TTW (Veni-Project 13669), a part of NWO; the Erasmus MC Foundation; the Phospholipid Research Center, Heidelberg, Germany; and the Thoraxcenter of Erasmus MC. The authors thank Gert van Cappellen and Adriaan Houtsmuller from the Erasmus MC Optical Imaging Center; Willem J. B. van Wamel from the Department of Medical Microbiology and Infectious Diseases, Erasmus MC; and Alessandra Scarpellini from Nikon Instruments Europe for the fruitful discussions.

REFERENCES

Baumgart T, Hunt G, Farkas ER, Webb WW, Feigenson GW. Fluorescence probe partitioning between Lo/Ld phases in lipid membranes. Biochim Biophys Acta Biomembr 2007;1768:2182–2194.

Binsalamah ZM, Paul A, Prakash S, Shum-Tim D. Nanomedicine in cardiovascular therapy: Recent advancements. Expert Rev Cardiovasc Ther 2012;10:805–815.

Chen X, Wang J, Versluis M, de Jong N, Villanueva FS. Ultra-fast bright field and fluorescence imaging of the dynamics of micrometer-sized objects. Rev Sci Instrum 2013;84 063701.

Chen X, Leow RS, Hu Y, Wan JMF, Yu ACH. Single-site sonoporation disrupts actin cytoskeleton organization. J R Soc Interface 2014;11 20140071.

Chin CT, Lancée C, Borsboom J, Mastik F, Frijlink ME, De Jong N, Versluis M, Lohse D. Brandaris 128: A digital 25 million frames per second camera with 128 highly sensitive frames. Rev Sci Instrum 2003;74:5026–5034.

De Cock I, Zagato E, Braeckmans K, Luan Y, de Jong N, De Smedt SC, Lentacker I. Ultrasound and microbubble mediated drug delivery: Acoustic pressure as determinant for uptake via membrane pores or endocytosis. J Control Release 2015;197:20–28.

De Cock I, Lajoinie G, Versluis M, De Smedt SC, Lentacker I. Sonoprinting and the importance of microbubble loading for the ultrasound mediated cellular delivery of nanoparticles. Biomaterials 2016;83:294–307.

Emmer M, Vos HJ, Versluis M, de Jong N. Radial modulation of single microbubbles. IEEE Trans Ultrason Ferroelectr Freq Control 2009;56:2370–2379.

Fan Z, Liu H, Mayer M, Deng CX. Spatiotemporally controlled single cell sonoporation. Proc Natl Acad Sci USA 2012;109:16486–16491.

Gelderblom EC, Vos HJ, Mastik F, Faez T, Luan Y, Kokhuis TJA, Van Der Steen AFW, Lohse D, De Jong N, Versluis M. Brandaris 128 ultra-high-speed imaging facility: 10 years of operation, updates, and enhanced features. Rev Sci Instrum 2012;83 103706.

Goh BHT, Conneely M, Kneuper H, Palmer T, Klaseboer E, Khoo BC, Campbell P. High-speed imaging of ultrasound-mediated bacterial Biofilm Disruption. IFMBE Proc 2015;45:533–536.

Helfield BL, Cherin E, Foster FS, Goertz DE. Investigating the subharmonic response of individual phospholipid encapsulated microbubbles at high frequencies: A comparative study of five agents. Ultrasound Med Biol 2012;38:846–863.

Helfield B, Chen X, Watkins SC, Villanueva FS. Biophysical insight into mechanisms of sonoporation. Proc Natl Acad Sci USA 2016;113:9983–9988.

Helfield BL, Chen X, Qin B, Watkins SC, Villanueva FS. Mechanistic insight into sonoporation with ultrasound-stimulated polymer microbubbles. Ultrasound Med Biol 2017;43:2678–2689.

Hu Y, Wan JMF, Yu ACH. Membrane perforation and recovery dynamics in microbubble-mediated sonoporation. Ultrasound Med Biol 2013;39:2393–2405.

Hu J, Zhang N, Li L, Ma Y, Zhao C, Wu Q, Li Y, He N, Wang X. The synergistic bactericidal effect of vancomycin on UTMD treated biofilm involves damage to bacterial cells and enhancement of metabolic activities. Sci Rep 2018;8:192.

Jia C, Xu L, Han T, Cai P, Yu ACH, Qin P. Generation of reactive oxygen species in heterogeneously sonoporated cells by microbubbles with single-pulse ultrasound. Ultrasound Med Biol 2018;44:1074–1085.

Kooiman K, Foppen-Harteveld M, van der Steen AFW, de Jong N. Sonoporation of endothelial cells by vibrating targeted microbubbles. J Control Release 2011;154:35–41.

Kooiman K, Kokhuis TJA, van Rooij T, Skachkov I, Nigg A, Bosch JG, van der Steen AFW, van Cappellen WA, de Jong N. DSPC or DPPC as main shell component influences ligand distribution and binding area of lipid-coated targeted microbubbles. Eur J Lipid Sci Technol 2014a;116:1217–1227.

Kooiman K, Vos HJ, Versluis M, de Jong N. Acoustic behavior of microbubbles and implications for drug delivery. Adv Drug Deliv Rev 2014b;72:28–48.

Kooiman K, Van Rooij T, Qin B, Mastik F, Vos HJ, Versluis M, Klibanov AL, De Jong N, Villanueva FS, Chen X. Focal areas of increased lipid concentration on the coating of microbubbles during short tone-burst ultrasound insonification. PLoS One 2017;12 e0180747.

Kwan JJ, Borden MA. Lipid monolayer collapse and microbubble stability. Adv Colloid Interface Sci 2012;183−184:82–99.

Lammertink BHA, Deckers R, Derieppe M, De Cock I, Lentacker I, Storm G, Moonen CTW, Bos C. Dynamic fluorescence microscopy of cellular uptake of intercalating model drugs by ultrasound-activated microbubbles. Mol Imaging Biol 2017;19:683–693.

Lentacker I, Wang N, Vandenbroucke RE, Demeester J, De Smedt SC, Sanders NN. Ultrasound exposure of lipoplex loaded microbubbles facilitates direct cytoplasmic entry of the lipoplexes. Mol Pharm 2009;6:457–467.

Lentacker I, Geers B, Demeester J, De Smedt SC, Sanders NN. Design and evaluation of doxorubicin-containing microbubbles for ultrasound-triggered doxorubicin delivery: Cytotoxicity and mechanisms involved. Mol Ther 2010;18:101–108.

Lentacker I, De Cock I, Deckers R, De Smedt SC, Moonen CTW. Understanding ultrasound induced sonoporation: Definitions and underlying mechanisms. Adv Drug Deliv Rev 2014;72:49–64.

Luan Y, Lajoinie G, Gelderblom E, Skachkov I, van der Steen AFW, Vos HJ, Versluis M, De Jong N. Lipid shedding from single oscillating microbubbles. Ultrasound Med Biol 2014;40:1834–1846.

Maresca D, Emmer M, van Neer PLMJ, Vos HJ, Versluis M, Muller M, de Jong N, van der Steen AFW. Acoustic sizing of an ultrasound contrast agent. Ultrasound Med Biol 2010;36:1713–1721.

Qin P, Han T, Yu ACH, Xu L. Mechanistic understanding the bioeffects of ultrasound-driven microbubbles to enhance macromolecule delivery. J Control Release 2018;272:169–181.

van der Meer SM, Dollet B, Voormolen MM, Chin CT, Bouakaz A, de Jong N, Versluis M, Lohse D. Microbubble spectroscopy of ultrasound contrast agents. J Acoust Soc Am 2007;121:648–656.

van Rooij T, Skachkov I, Beekers I, Lattwein KR, Voorneveld JD, Kokhuis TJA, Bera D, Luan Y, van der Steen AFW, de Jong N, Kooiman K. Viability of endothelial cells after ultrasound-mediated sonoporation: Influence of targeting, oscillation, and displacement of microbubbles. J Control Release 2016;238:197–211.

van Wamel A, Kooiman K, Harteveld M, Emmer M, ten Cate FJ, Versluis M, de Jong N. Vibrating microbubbles poking individual cells: Drug transfer into cells via sonoporation. J Control Release 2006;112:149–155.

Westein E, Flierl U, Hagemeyer CE, Peter K. Destination known: Targeted drug delivery in atherosclerosis and thrombosis. Drug Dev Res 2013;74:460–471.